UNIVERSITAT POLITÈCNICA DE VALÈNCIA

ESCUELA TÉCNICA SUPERIOR INGENIEROS INDUSTRIALES VALENCIA

Select degree

VOXEL-WISE ANALYSIS OF TRACTOGRAPHY DATA TO IMPROVE CLUSTERING OF FIBER GEOMETRIES

Blanca Bastardés Climent

REVIEWER: Örjan Smedby

Select: Rodrigo Moreno

Academic year: 2018-19

DEGREE PROJECT IN MEDICAL ENGINEERING,
SECOND CYCLE, 15 CREDITS
STOCKHOLM, SWEDEN 2019

Voxel-Wise Analysis of Tractography Data to Improve Clustering of Fiber Geometries

BLANCA BASTARDÉS CLIMENT

KTH ROYAL INSTITUTE OF TECHNOLOGY
SCHOOL OF ENGINEERING SCIENCES IN CHEMISTRY, BIOTECHNOLOGY AND HEALTH

Voxel-wise Analysis of Tractography Data to Improve Clustering of Fiber Geometries

BLANCA BASTARDÉS CLIMENT

Bachelor in Medical Engineering
Date: Friday 8th February, 2019
Supervisor: Rodrigo Moreno
Reviewer: Örjan Smedby
Examiner: Mats Nilsson
Swedish title: Voxelvis analys av traktografiska data för att förbättra kluster av fibergeometrier.
School of Technology and Health

Abstract

Many neurodegenerative brain pathologies are closely tied to white matter degeneration which develops alterations in water diffusion at the tissue. For this reason, it becomes essential to study the neural connections in order to improve diagnosis and treatment of brain diseases. Tractography is a non-invasive technique that allows the visualization of white matter tracts in-vivo from diffusion Magnetic Resonance Imaging (MRI). However, there are many differences between results due to the lack of a standardized methodology or automatic procedures to follow. The aim of this project is to set a procedure with specific probabilistic methods to perform an optimal estimation of white matter fiber orientations within each voxel, even at confusing regions where crossing fibers are present. This procedure will be used to create a dataset that will be used in the future to generate population atlases, which will be not only clinically helpful to evaluate possible anatomical alterations in the brain but also in refinement of tractography results. The tractography was performed using High Angular Resolution Diffusion Imaging (HARDI) of healthy subjects. The number of tracts selected to generate the tractogram was 10 million. Geometrical features were extracted for each voxel from three different regions of the whole tractogram. The location of the regions was decided based on the number of fibers present. This information was extracted from literature. Moreover, tractograms of 500.000 and 1.000.000 tracts were also generated. The method Spherical-Deconvolution Informed Filtering of Tractograms 2 (SIFT2) was applied to the three tractograms and its contribution was tested, but it barely changed the results. The relevance of the number of streamlines was also explored. 1.000.000 streamlines were found to be a sufficient number. Finally, two different clustering methods were performed to distinguish the different fiber bundles present in each voxel, using the previous features. One of the clustering methods explored was the Mean Shift method which seems to be promising. However, to refine the accuracy of the results, distance measurement should be adapted, and a greater number of parameters considered, such as curvature.

Contents

Acronyms

ACT	Anatomical-Constrained Tractography
ADC	Apparent Diffusion Coefficient
CNS	Central Nervous System
CSD	Constrained Spherical Deconvolution
CSF	Cerebrospinal Fluid
dMRI	Diffusion Magnetic Resonance Imaging
DT	Diffusion Tensor
DW	Diffusion Weighted
FA	Fractional Anisotropy
FOD	Fiber Orientation Distribution
GM	Grey Matter
HARDI	High Angular Resolution Diffusion Imaging
MRI	Magnetic Resonance Imaging
MSMT-CSD	Multi-Shell Multi-Tissue Constrained Spherical Deconvolution
NMR	Nuclear Magnetic Resonance
RF	Radiofrequency
SIFT	Spherical-Deconvolution Informed Filtering of Tractograms
SIFT2	Spherical-Deconvolution Informed Filtering of Tractograms 2
WM	White Matter

Chapter 1

Introduction

Diffusion Magnetic Resonance Imaging (dMRI) is a noninvasive imaging method that allows the visualization and calculation of the diffusion of water molecules in biological tissues "in vivo". The water diffusion in the white matter (WM) of the brain is faster parallel to the axons than perpendicular because the molecules have to go through fewer obstacles [1]. For this reason, dMRI can provide voxel-wise information on the orientation of groups of neuronal axons, and thus on the structural connectivity between brain regions [2]. Moreover, by using high angular resolution diffusion imaging (HARDI), it is possible to extract more complex fiber configurations and model fiber trajectories by employing tractography methods.

The local orientation and geometry of tractography results derived from different subjects can be compared at corresponding anatomical locations to create human brain atlases, which can be used as a reference for different applications, such as the improvement of tractography algorithms themselves or the identification of abnormal pathological neuroanatomy [3][4][5][6]. Previous studies by Brusini et al. explored a novel approach for both characterizing the geometry of fibers at a voxel level and locally clustering them [7][8][9]. This approach consisted in describing the fiber's local geometries with both their Frenet-Serret frames and their curvature. This method was shown to achieve a good representation of well-known WM structures, to be usable for creating population atlases and to characterize regions with high similarity across subjects. However, these studies also highlighted some limitations of the current results, which are strongly dependent on many different parameters, such as the tractog-

raphy methods being used, the total number of tracts being modeled, the choice of the step-size for the tracking, as well as the preprocessing performed on the dMRI data. For this reason, there is a need to further investigate how the local representation of fibers changes depending on the chosen image processing pipelines.

1.1 Purpose and objectives

This final project is a continuation of the work carried out by Irene Brusini in 2016 for her Master's thesis project in the Division of Biomedical Imaging of the KTH Royal Institute of Technology (Stockholm, Sweden).

The main aim of this proposed thesis project is to create a procedure to perform an optimal estimation of fiber bundles at a voxel level by testing different dMRI image processing methods, as well as different tractography algorithms and settings. Such dataset is then going to be an extremely useful resource for the creation of population level atlases that aim at representing fiber geometries at a voxel level. To achieve that main objective, it was necessary to break it down into a series of specific tasks:

1. Literature study on state-of-the-art dMRI image processing and tractography methods.
2. Analysis of the tools that are implemented in the software package MRtrix (www.mrtrix.org) and choice of the most suitable method to be tested (considering both quality in the results and time limitations).
3. Design of a registration procedure of the subjects from the available Human Connectome Project dataset [10].
4. Understanding the SIFT2 method and test it with the subjects.
5. Determining a suitable clustering method to differentiate the fiber bundles at each voxel.
6. Evaluating the results and critical selection of the most reliable data.

Chapter 2

State of the art

2.1 Neuroscience

The Central Nervous System (CNS), which includes the brain and spinal cord, is made up of many different types of cells, but the primary functional unit is a cell called neuron. Neurons are responsible for the transmission of nerve impulses. A neuron is composed of a cell body and two types of ramifications: dendrites and axon. The cell body is where the nucleus and cytoplasm of the cell are, the dendrites are short tree branches where a neuron receives input from other cells, and the axon is a long, thin structure coated with myelin sheath that corresponds with the transmitting part of the neuron. Myelin is a substance with low diffusive properties which guarantees the transmission of the nerve impulse between neurons. Myelin sheaths are presented at regular intervals by the nodes of Ranvier, helping to accelerate the propagation of nervous flux. The axonal termination contacts the dendrites or cell bodies of other neurons, creating a synapse [11].

The brain is part of the CNS and the most complex part of the human body. It is composed of three different tissue types: white matter (WM), grey matter (GM) and cerebrospinal fluid (CSF). WM is the part mainly composed of myelinated fibers and responsible for interconnecting different regions of GM. The GM is where the neuronal somas, dendrites, ending axons and capillaries are. It envelopes WM and corresponds to the most complex organization of the entire ner-

vous system. The CSF is filtered blood plasma that protects, sustains and nourishes the whole system.

Due to the essential role that WM plays being responsible for the interconnectivity, many studies have been developed to study the connectivity pattern of the brain, following the myelin nerve fibers called neural fiber bundles.

2.2 Introduction to magnetic resonance imaging

Magnetic Resonance Imaging (MRI) is a non-invasive medical imaging technique that offers the study of the interior of the human body, with a high spatial resolution and excellent contrast for soft tissues. It is based on the principle of the Nuclear Magnetic Resonance (NMR).

NMR relies on the quantum properties of atomic nuclei, evaluating the reaction of the hydrogen nuclei when an atom is subjected to a magnetic field B_0. The nuclei are constantly rotating around their axis behaving like small magnets. Because the directions of the axis are randomly distributed, there is a null magnetization of the body due to the mutual cancellation of the magnetic fields generated by the protons. Nuclei under B_0 will have a reorientation of their axis to the direction of the magnetic field. The frequency at which the nuclei do the precession movement around the axis of the magnetic field is known as the Larmor frequency (equation 2.1). Such frequency depends on the gyromagnetic radius γ of each atom and is proportional to the magnetic field.

$$\omega_0 = \gamma B_0 \tag{2.1}$$

Since nuclei will be all aligned, the magnetic field they generate will not be null anymore resulting in a global magnetization M along the longitudinal axis, and null along the transverse. This is the moment when a radiofrequency (RF) pulse, with the same frequency as the Larmor frequency, is sent so that nuclei come into resonance and change their spin direction. This will start a transverse magnetization and it is called the excitation phase. When the pulse is over, the relax-

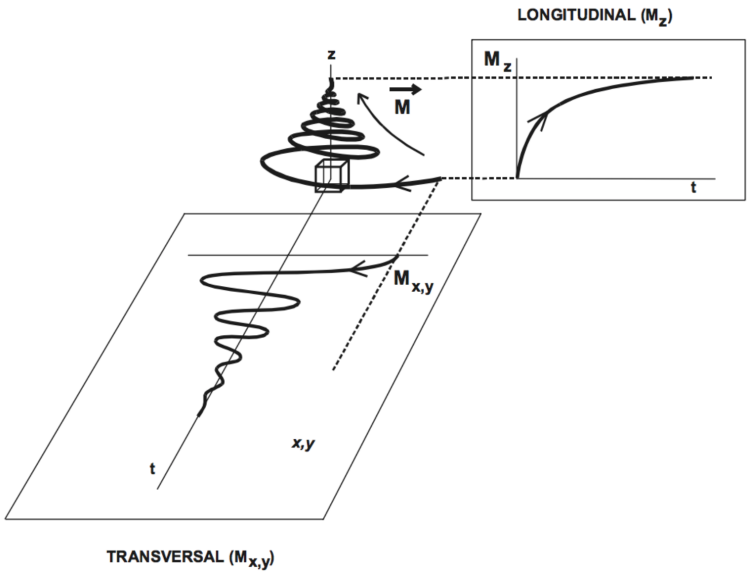

Figure 2.1: Study of the Relaxation following the evolution in time of the longitudinal component M_z and of the transverse component $M_{x,y}$. (Source: Gili [12]).

ation phase starts, and nuclei begin to "relax". There are two types of relaxation. T1 relaxation, when nuclei at a high energy state go back to the low energy state, recovering the magnetization in the direction of the magnetic field. T1 corresponds to the longitudinal relaxation and it is the time constant in milliseconds that takes for Magnetization to recover 63% of its value. Each voxel will present a T1 depending on the free water it contains. The lower the value of T1, the faster the equilibrium state is reached, which means that the relaxation is faster. Therefore, a short T1 corresponds to a rapid release of energy. T2 relaxation corresponds to the relaxation in the transverse axis due to the loss of phase of the precessing nuclei, losing magnetization along this axis. T2 is the time it takes for the transverse magnetization to lose 63% of its value. T2 relaxation is much faster than T1 relaxation. [12][13].

2.3 Diffusion MRI

The principle of diffusion is the microscopic movement of atoms and molecules in solution or gas. In human tissues, predominant

molecules that flow freely around are water molecules.

Diffusion Imaging quantifies molecular diffusion restriction in the body by the detection of the signal emitted from the hydrogen nucleus of the water molecules after applying a rephasing pulse.

2.3.1 Diffusion of water molecules

Two different types of diffusion can be differentiated. Isotropic diffusion, when molecules of hydrogen are free to move to any direction without restriction. It is the same in all directions. In addition, there is anisotropic diffusion when water molecules are restricted by some obstacle resulting an asymmetric movement. It is not the same in all directions [14].

2.3.2 Acquisition

The diffusion is measured by the attenuation of the signal when the water molecules move in a region under a magnetic field gradient. For that it is used the Stejskal-Tanner sequence. It is based on the conventional sequence spin-echo T2w, which is a 90º RF pulse followed by another pulse of 180º, plus a symmetric pair of gradients in opposite polarity, before and after the 180º pulse.

After the 90º RF pulse, molecules get the same phase. The first gradient produces a dephasing of the water molecules that the second gradient after the 180º RF pulse will rephase only for the protons that have the same position as before the first gradient. In this way, the signal will be lost in the locations of all the other protons that have not been rephased so that the others will lose signal.

2.3.3 Diffusion Tensor Imaging

The quantification of the diffusion is done by the following formula:

$$I = I_0 e^{-bD} \tag{2.2}$$

and the signal decreases according to b:

$$b_i = \gamma^2 G_i^2 \gamma^2 (\Delta - \frac{\delta}{3}) \tag{2.3}$$

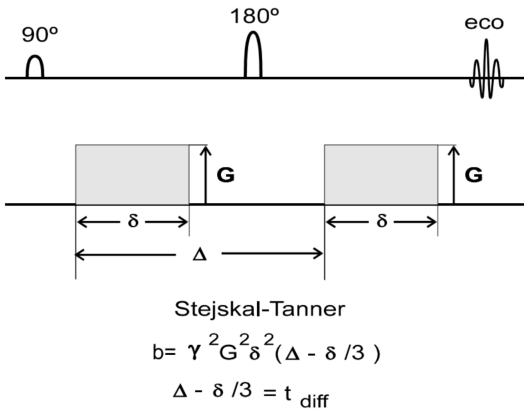

Figure 2.2: Stejskal-Tanner sequence diagram for the diffusion calculation. It depends on the duration of the gradient δ, the gradient amplitude G and the interval between the diffusion gradients Δ. δ and Δ determine the time during which diffusion is measured t_{diff}. (Source: Gili [12]).

For short periods of time the above-presented quantification is good enough but for long ones the Apparent Diffusion Coefficient (ADC) should be taken into account. ADC measures diffusion in one direction and results from the combination of a weighted diffusion image and a reference one, so that

$$ADC = -\frac{\ln \frac{DWI}{T2}}{b} \tag{2.4}$$

In order to evaluate diffusion in 3D images a Diffusion Tensor (DT) of ADC is developed. At least 6 different acquisition directions will be required resulting a 3x3 matrix:

$$\vec{D} = \begin{bmatrix} D_{xx} & D_{xy} & D_{xz} \\ D_{yx} & D_{yy} & D_{yz} \\ D_{zx} & D_{zy} & D_{zz} \end{bmatrix}$$

When elements outside the diagonal are zero, it means that there is an alignment with the principal axis of the diffusion due to the absence of correlation with the displacements in the orthogonal directions. Therefore, the eigenvalues will be the principal axis and the eigenvectors will be parallel to the direction of the brain fibers.

Different parameters can be extracted from the DT. The principal eigenvector will represent the direction of the water molecules' diffusion, i.e. the principal directions of the fibers in a voxel. The second and third eigenvectors correspond to the diffusion along the transverse plane to the fascicles [15].

Diffusion average is computed by the three different eigenvalues and determines the average water diffusivity at a voxel level.

$$D_{av} = \frac{\lambda_1 + \lambda_2 + \lambda_3}{3} \tag{2.5}$$

Fractional Anisotropy (FA) is an index that measures the degree of direction of diffusivity within a voxel. When the value is high it means that there is one prevalent diffusion direction, conforming an elongation of the diffusion ellipsoid, due to the presence of a tract of white matter.

$$FA = \sqrt{\frac{(\lambda_1 - \lambda_2)^2 + (\lambda_2 - \lambda_3)^2 + (\lambda_3 - \lambda_1)^2}{2((\lambda_1)^2 + (\lambda_2)^2 + (\lambda_3)^2}} \tag{2.6}$$

However, the DT model has a relevant limitation which is that it is only capable of representing a unique orientation of the fibers in each voxel, which is represented by the main eigenvector of the tensor [15]. For this reason, it will not be able to properly estimate regions where crossing fibers are present. This will lead to a poor representation of the real anatomical structure and the estimation of fiber pathways could become erroneous.

2.3.4 HARDI

High Angular Resolution Diffusion Imaging (HARDI) was developed to discriminate multiple fibers crossing the same voxel since DT can only resolve one single direction. It estimates the value of ADC according to the coded angle using the method of decomposition for spherical harmonics to determine the complex diffusion profiles. Many HA- RDI based methods have been developed in order to overcome the fiber crossing limitation [16].

The Constrained Spherical Deconvolution (CSD) algorithm estimates the distribution of the fiber orientations present within each voxel without any assumption regarding the number of fiber populations present. The Diffusion Weighted (DW) signal attenuation measured can be represented as the spherical convolution of the response function of the fiber population in each voxel with the Fiber Orientation Distribution (FOD). Therefore, the FOD can be estimated by the inverse operation, i.e. the deconvolution from the measured DW signal [17].

The order of water molecules displacement expected in a diffusion weighted study is 10 μm so that it can be assumed that there will not be any water exchange between fiber bundles. Additionally, for curved fibers, it will be assumed that there will not be any exchange between orientational sections of each fiber bundle. Therefore, the diffusion weighted signal can be represented by the sum of the signals from each orientational regions in each population.

Tournier's method [2] relies on the assumption that the DW signal attenuation from a single coherently oriented fiber population can be represented by an axially symmetric response function $R(\theta)$, θ being the elevation angle in spherical coordinates. Therefore, the measured signal can be represented as the convolution over the unit sphere of $R(\theta)$ with the FOD $F(\theta, \phi)$, where $F(\theta, \phi)$ corresponds to the fraction of aligned fibers along the direction (θ, ϕ) (see Figure 2.3):

$$S(\theta, \phi) = F(\theta, \phi) \circledast R(\theta) \tag{2.7}$$

The spherical convolution operations can be easily obtained by simple matrix multiplications. The nth order spherical harmonic representation of $S(\theta, \phi)$ can be formulated as:

$$S^n = R^n F^n \tag{2.8}$$

R^n and F^n are a matrix and a vector representing the nth order rotational and spherical harmonic decomposition of $R(\theta)$ and $F(\theta, \phi)$, respectively.

One of the advantages of this method when estimating the response function is that it does not rely on any diffusion model, whereas the DT model does. It is estimated from the data by mea-

Figure 2.3: Representation of the spherical deconvolution principle when two fiber orientations are crossing. The DW signal attenuation can be expressed as the convolution over the unit sphere of the response function $R(\theta)$ and the FOD $F(\theta, \phi)$. (Source: Tournier et al. [2] with permission from Elsevier).

suring the DW signal profile in regions that are likely to contain only one fiber population.

The CSD method has been proved to be simple and fast. Its operations are linear so that the noise propagation can be easily inferred, being then, a relatively robust method to noise. However, the susceptibility to noise increases when using high order harmonics. It is model-independent and no prior knowledge on the number of fiber orientations is needed [2].

2.4 Tractography

Several high-order methods were developed with the aim of estimating fiber bundle orientations in each voxel due to the poor representation of the white matter structure that DT offers in regions with crossing fibers. Behrens et al. [18] published that around one third of White Matter (WM) voxels have that complex structure. In contrast, Jeurissen et al. [19] stated that it is around 90 $\%$.

Tractography is a 3D modelling technique that uses dMRI data to represent fiber bundles in the brain from the directions of diffusion. There are three main categories of fiber-tracking algorithms: deterministic, probabilistic and global tractography algorithms. They have different ways to determine the streamline trajectories. Deterministic algorithms usually follow the most likely fiber orientation per voxel whereas probabilistic methods consider more orientations at a local level, i.e. not only they look for the main direction but also explore

other ones. It is true that deterministic approaches lead to a more realistic results, but they can also fail to reconstruct connections between distant regions with small quantity of noise. In contrast, probabilistic ones are better when it comes to crossing fibers, but they are slower. Both types are local reconstruction methods analyzing voxels and their neighbourhood. Instead, global tractography is based on the generation of a full track that best represents the measured DW data. It is less susceptible to noise, but it does not consider anatomical priors and therefore, it will not be as accurate as the other two [20].

2.4.1 Anatomically-Constrained Tractography

Independently of the tracking method chosen, streamlines tractography also has some limitations that can affect the reliability of the reconstructed fiber connections. In [21] the importance of the termination points of the streamlines is widely explained. There are different methods to determine the end of a streamline by thresholding different parameters, but they all result imperfect.

Anatomical-Constrained Tractography (ACT) is an additional method to streamlines tractography that makes use of prior anatomical knowledge and/or structural information to guide the tractography process, preventing from some false positives associated to some tractography methods. Instead of defining a binary mask to be used for the tracking, biological properties of the different tissues of the brain will also be considered. Segmentation and classification of the tissues is needed and will then be represented as estimated partial volume fraction maps so that ACT will become independent of the chosen segmentation method [21].

Note that the direction of the tracking is not influenced since this is provided by the diffusion model. But what is influenced is both the termination and acceptance of a streamline. Specific criteria were determined for streamline projections. For instance, most of the streamline endpoints should be expected at the GM since this is the tissue where the interconnection between axon bundles occurs. Therefore, a streamline should never end at WM tissue and never enter the CSF. Assuming this, when a streamline reaches GM it will be an appropriate termination point and if it enters Cerebrospinal Fluid (CSF) it will be rejected. Anatomical information was also used to determine seeding criteria

such as WM-seeding, Grey Matter (GM)-seeding, back-tracking and minimum length [21].

2.4.2 Spherical-deconvolution Informed Filtering of Tractograms

ACT allows us to perform a more accurate reconstruction of the fiber bundles, however there are still some biases that could affect the reliability of the method. In [22] a retrospective filtering method was proposed in order to improve the reconstructions, called Spherical-Deconvolution Informed Filtering of Tractograms (SIFT). Its aim is to find a subset of streamlines that best matches the diffusion signal. It relies on the spherical deconvolution of the signal in order to select which streamlines should be removed. This filtering operation leads to a decrease of the biases and an increase of plausibility.

To evaluate the accuracy of the reconstructions, the proportionality coefficient μ is used. It compares the streamline density of each FOD lobe by assigning a value with the integral of that lobe.

$$TD_l = \sum_{s:|s_l|>0} |s_l| \tag{2.9}$$

$$\mu = \frac{\sum_{l=1}^{L}(PM_l \cdot FD_l)}{\sum_{l=1}^{L}(PM_l \cdot TD_l)} \tag{2.10}$$

For each voxel, the FD_l is the FOD integral of lobe number l whereas TD_l is the track density of that lobe which depends on the length of the streamline attributed to that lobe s_l (see equation (2.9)). PM_l is the value of the processing mask in the voxel where the lobe is located.

Due to the possible presence of biases during the reconstruction, a cost-function f was defined to quantify the accuracy of the reconstruction with the underlying diffusion data.

$$f = \sum_{V}(PM_V \sum_{l=1}^{L}(\mu TD_l - FD_l)^2) \tag{2.11}$$

When a streamline is removed, the model will be affected in two different ways. Not only TD_l will be reduced but also the proportionality coefficient μ will be increased and, therefore, the cost function will be influenced as well. And that is the reason why the SIFT2 method was developed [23].

In the SIFT2 method, the proportionality coefficient μ remains the same but the density at each lobe is computed differently, considering variable contribution weights from individual streamlines.

$$TD_l = \sum_{s:|s_l|>0} |s_l| \cdot e^{F_s} \tag{2.12}$$

F_s is the weighting coefficient for each streamline s and e^{F_s} is the weighting factor.

The aim of this method is to find a vector of weighting coefficients F_s so that the streamlines will contribute to the density calculation in order to match the densities with the FOD lobe integrals. The new cost-function is then,

$$f = \sum_{V}[(PM_V \sum_{l=1}^{L}(\mu TD_l - FD_l)^2)] + A\lambda_{reg} \sum_{s=1}^{N}[f_{reg}(s)] \tag{2.13}$$

where there is the additional regularization term f_{reg} with A as a scaling parameter to compare different imaging and reconstruction parameters by the user-controllable parameter λ_{reg}. In [23] two different regularization were tested, the conventional Tikhonov and the advanced akin to total variation (TV).

The SIFT2 algorithm has been proved to be more beneficial than the original one since it retains the entire tractogram for further processing. It is not dependent on removing streamlines and the fact of having a regularization parameter gives more control to the reconstruction. The existence of the new method does not mean that the original one is not applicable anymore and it is also believed that the combination of the two methods could be beneficial [23].

2.5 Clustering

Tractography data is composed by big sets of streamlines. For this reason, in order to group the streamlines into fiber bundles it is necessary to draw on automated methods [24].

Clustering is a type of data analysis that tries to find natural groups of data, so that the data points grouped together are more similar to each other than those of the other groups. Three main categories of clustering methods can be found: Distance-based, density-based and distribution-based. On one hand, distance-based clustering methods try to find the best way to group data in order to maximize the inter-cluster distances and minimize the intra-cluster distances. Hierarchical clustering belongs to this category and it relies on dendrograms, tree diagrams representing relationships between similar sets of data. On the other hand, density-based clustering methods try to find the regions of higher densities, which could correspond to a cluster. For instance, Mean Shift clustering is a technique that supposes that all data points represent a part of an underlying probability density function, and shifts the samples to the regions with higher density. Additionally, distribution-based clustering methods aim to find the best parameters of a statistical underlying model to best describe the data. An example for this category is Expectation-Maximization algorithm [25].

Chapter 3

Methods

In this chapter, the methods used to analyze and generate tractography data as well as the ones tested for the clustering of fiber geometries are described. From the raw data from the 1200 Subjects HCP Database [10], fiber directions and tractography data were estimated. Results were filtered and geometrical features were extracted so that fibers could be clustered at a voxel level. Figure 3.1, shows the pipeline followed.

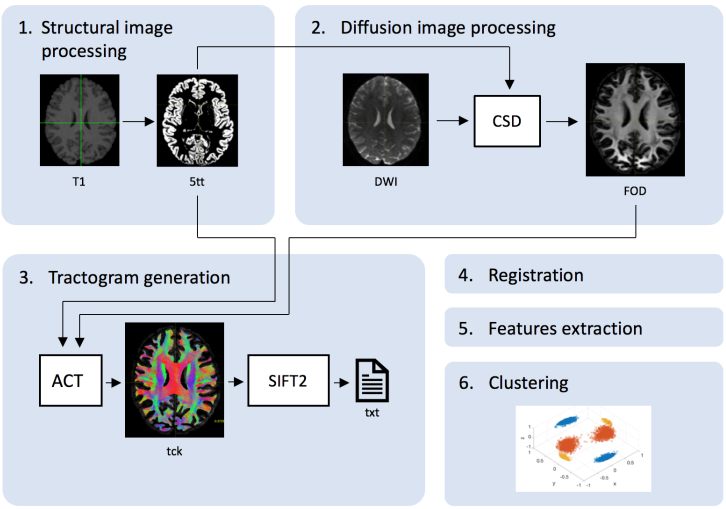

Figure 3.1: Pipeline followed in this project. 1. Generation of 5-tissue segmentation image. 2. Estimation of FOD with CSD. 3. Tractogram generation with ACT and filtering with SIFT2. 4. Registration to MNI. 5. Tractogram features extraction and 6. Clustering with features and SIFT2 weights.

3.1 Dataset

In this study, data was selected from the 1200 Subjects Data Release of the Human Connectome Project (HCP), including 1206 healthy young adult participants collected in 2012-2015. Structural images (T1w and T2w) and diffusion images (HARDI) were the modalities used. HARDI data have TR = 5520 ms, TE = 89.5 ms, 270 gradient directions with 3 shells of b = 1000, 2000, and 3000 s/mm^2, 18 non-diffusion-weighted images (b = 0) with isotropic image resolution of 1.25 mm.

The study was applied to three specific regions of the brain according to the number of the fiber orientations present. The regions are the corpus callosum (one orientation), the intersection of the corticospinal tract and the pontine crossing tract (two orientations) and the intersection of the corona radiata, the superior longitudinal fasciculus and the corpus callosum (three orientations) [8].

3.2 Tractography

Tractography data was provided by Wasserthal, Neher, and Maier-Hein [26], who had already performed a study in which white matter tracts were segmented in a fast and accurate way from the subjects of the above-mentioned database.

In order to generate the whole-brain tractograms, advanced tools for the analysis of diffusion MRI data were used from the free available software MRtrix [27]. The following commands were used to obtain the whole-brain tractograms:

```
#Generate a tissue-segmented image
5ttgen fsl T1w_acpc_dc_restore_brain.nii.gz 5TT.mif -
    premasked
#Estimate the multi-shell, multi-tissue response functions
dwi2response msmt_5tt Diffusion.nii.gz 5TT.mif RF_WM.txt
    RF_GM.txt RF_CSF.txt -voxels RF_voxels.mif -fslgrad
    Diffusion.bvecs Diffusion.bvals
#Perform Multi-Shell, Multi-Tissue CSD
dwi2fod msmt_csd Diffusion.nii.gz RF_WM.txt WM_FODs.mif RF_GM
    .txt GM.mif RF_CSF.txt CSF.mif -mask nodif_brain_mask.nii.
    gz -fslgrad Diffusion.bvecs Diffusion.bvals
```

```
#Generate the tractogram
tckgen -algorithm iFOD2 WM_FODs.mif All_10M.tck -act 5TT.mif
    -backtrack -crop_at_gmwmi -seed_image nodif_brain_mask.nii
    .gz -maxlength 250 -minlength 40 -number 10M -cutoff 0.06
    -maxnum 0
```

3.2.1 Multi-Shell Multi-Tissue (MSMT) CSD algorithm

For tractography, Multi-Shell Multi-Tissue Constrained Spherical Deconvolution (MSMT-CSD) method [28] was used to extract a multi-tissue FOD.

To apply this algorithm, a segmentation of the different tissues is required in order to define a whole-brain mask where to estimate the response function of each. A maximum spherical harmonic order l_{max} = 8 and a combination of 3 shells of b = 1000, 2000, and 3000 $\mathrm{s/mm^2}$ were used. The resulting FOD information was then used with a suitable fiber-tracking algorithm in order to infer the connectivity.

3.2.2 Anatomically-Constrained Tractography

Fiber directions were determined with ACT and the iFOD2 algorithm (see section 2.4.1). The maximum length of tracks was set to 250 mm and the minimum to 40 mm. The number of fibers generated was 10 million and seed streamlines were placed randomly within the mask image.

This algorithm considers the biological properties of the tissue types and fluid within the brain, as well as the nature of the axons of the WM that we are attempting to reconstruct [21]. The direction of tracking is not influenced. However, the mechanisms to determine the termination and acceptance or rejection of the streamlines are influenced. Due to the presence of the axonal bundles in WM which are responsible for the connections between GM areas, we should expect most of the endpoints when they reach GM. Backtracking allows tracks to be truncated and re-tracked if a poor structural termination is encountered. In this study, backtracking was performed to crop the streamlines' endpoints more precisely as they cross the GM-WM interface.

3.2.3 Filtering: SIFT2

Once the FOD and the tracking had been generated, SIFT2 (see section 2.4.2) was applied to filter the whole-brain fiber-tracking dataset such that the streamline densities matched the FOD lobe integrals.

```
#Filter the tractogram
tcksift2 All_10M.tck WM_FODs.mif out_weights
```

When using SIFT2, a text file is created instead. Each line of that text file corresponds with the weights e^{F_s} of each streamline s and will be used as a complement of the original tracking file for the reconstruction [23].

3.3 Registration

Since the images must belong to a common coordinate system to be able to compare results between subjects at a local level, a normalization to MNI space was chosen. This was done by applying transformations from specific warpings provided with the data, to both FODs and trackings.

Note that the deformation files that HCP provides, have the x component inverted, therefore a preliminary step to flip such axis was required to get the right results.

```
#Invert the x coordinate of the warping field
mrconvert acpc_dc2standard.nii.gz tmp-[].nii
mv tmp-0.nii x.nii
mrcalc x.nii -neg tmp-0.nii
#Convert displacement to deformation as required by mrtrix
warpconvert tmp-[].nii -type displacement2deformation
    warp_acpc2std.nii.gz
#Apply the transformation
mrtransform WM_FODs.mif warp_acpc2std.nii.gz WM_FODs_MNI.mif
```

```
#Invert the x coordinate of the warping field
mrconvert standard2acpc_dc.nii.gz tmp-[].nii
mv tmp-0.nii x.nii
mrcalc x.nii -neg tmp-0.nii
```

```
#Convert displacement to deformation as required by mrtrix
warpconvert tmp-[].nii displacement2deformation warp_std2acpc
    .nii.gz
#Apply the transformation
tcktransform All_10M.tck warp_std2acpc.nii.gz All_10M_MNI.tck
```

After the registration of all data to the MNI space, a binary mask was created and used to select the information belonging to the three regions of interest and filter out the information that does not belong to them.

3.4 Features Extraction

Once the FODs and the trackings are registered, the method of Brusini et al. [7] will be performed in order to extract geometrical features of the tracts that cross the selected areas in each subject. For every point P_i of a tract, the tangent vector T, binomial vector B and angle of curvature Θ were extracted according to:

$$T = \frac{P_{i+1} - P_{i-1}}{\|P_{i+1} - P_{i-1}\|} \tag{3.1}$$

$$B = \frac{v_1 \times v_2}{\|v_1 \times v_2\|} \tag{3.2}$$

$$\Theta = \arctan(\frac{\|v_1 \times v_2\|}{v_1 \cdot v_2}) \tag{3.3}$$

v_1 and v_2 are vectors corresponding to two successive track segments, delimited by the pairs $P_i - 1$, P_i and P_i, $P_i + 1$, respectively.

The mean of all the triplets (T, B, Θ) associated to the tract's points in each specific voxel results in the final voxel-wise characterization of a tract.

3.5 Fiber Clustering

The voxel-wise information obtained before is now going to be used to cluster the fibers into bundles. To reach that, in Brusini et al. [9] the

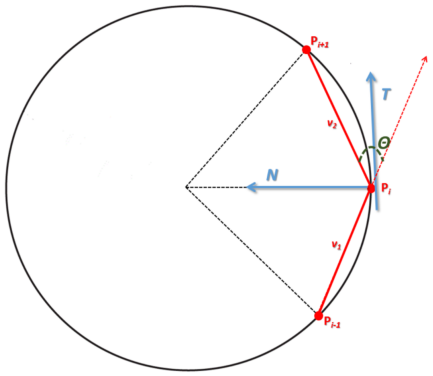

Figure 3.2: Representation of the geometrical features of one point P_i from a reconstructed fiber tract (solid lines in red). (Courtesy of Brusini [8]).

process was divided into two steps, one for distance measure and a second one for bundle clustering.

For the first one, distances between tracts were computed as in equation (3.4), F being the triplet (T, B, Θ) and N the normal vector defined as $(B \times T)$ of each tract. λ is a parameter to control the importance of the difference in curvature in the computation of the distance. It was set to $\lambda = 2$. Θ_{th} is an angle threshold to distinguish between low and high curvature cases so that when curvature of the two tracts is too low, the tangent will be mainly determining the distance, since B and N will be unstable. In contrast, if the tracts are bent, N will be the parameter that will best differentiate them (see Figure 3.3). Θ_{th} was set to 10º. For the second step, agglomerative hierarchical clustering was performed (see section 2.5). Data was divided into different groups according to the distance calculated in the previous step (see equation (3.4)). The criterion used to determine the optimal number of clusters was based on the one from Davies and Bouldin [29], which searches for the clustering solution with the minimum ratio of inter and intra-cluster distances.

$$D(F_1, F_2) = \begin{cases} 2\cos^{-1}\left(|T_1 \cdot T_2|\right) + \lambda|\Theta_1 - \Theta_2|, & \text{if } \min(\Theta_1,\Theta_2)<\Theta_{th} \\ 2\cos^{-1}\left(\frac{(|T_1 \cdot T_2| + |B_1 \cdot B_2| + |N_1 \cdot N_2|) - 1}{2}\right) + & \\ +\lambda\left|\theta_1 - (N_1 \cdot N_2) \cdot \Theta_2\right|, & \text{otherwise.} \end{cases} \tag{3.4}$$

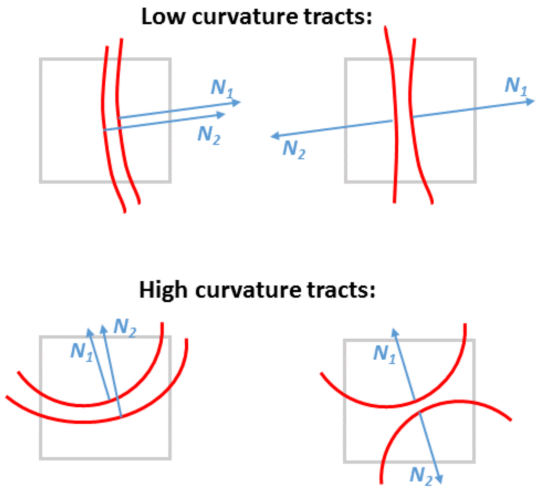

Figure 3.3: Representation of similarity tracts depending on the different curvature cases. If their curvature is low and their tangents are similar, the tracts will be considered similar even if the vectors N are parallel or opposite. If the curvature is high and they have similar tangents, only the ones with parallel vectors N will be treated as similar. (Courtesy of Brusini [8]).

The technique explained above was computed for 300.000 tracts per subject and resulted in promising results. However, since the number of modelled tracts in this study is 10 million and there were weights obtained from SIFT2 available, another clustering technique that could take those weights into account, such as Mean Shift [30], was also performed. It is a non-parametric density-based technique. For this method, only the tangent and the SIFT2 weights from all the parameters calculated were used.

The Mean Shift algorithm relies on kernel density estimation (KDE) (see section 2.5). Having weights for every point of each streamline a probability surface is generated. The kernel size is defined by the bandwidth so that the larger the bandwidth is, the wider the kernel size will be, and more points will belong to each cluster. It is an iterative method that is applied to every point making it climb up to the nearest peak on the KDE surface. The last iteration will be when the point converges. The original method uses a Gaussian kernel distribution for the distance estimation. However, in this study, the Von Mises–Fisher distribution is used to perform the clustering on a hypersphere:

$$f_p(\mathbf{x}; \boldsymbol{\mu}, \kappa) = C_p(\kappa) \exp\left(\kappa \boldsymbol{\mu}^T \mathbf{x}\right) \tag{3.5}$$

where $\mathbf{x}$ is a d-dimensional unit vector ($\mathbf{x} \in \mathbf{R}^d, \|\mathbf{x}\| = 1$), $\boldsymbol{\mu}$ is a unit vector orienting the center of the distribution, κ is a parameter to control the concentration of the distribution to the vector $\boldsymbol{\mu}$, and C is a normalization constant.

Chapter 4

Results

In the following chapter results of all the analysis decribed above are given.

4.1 Tractograms

Tractography data obtained by Wasserthal, Neher, and Maier-Hein [26] were explored at the three regions of interest. The tractograms were computed for 10 million streamlines. Information of the regions selected is given in Table 4.1. Figure 4.1 shows, for every region, the corresponding FODs lobes and the streamlines that cross the central voxel, proving that the tractogram follows the FODs directions.

Table 4.1: Regions of interest of the 10 million tractogram

Region	N Voxels	Central voxel	Avg. Streamlines/ voxel	Directions
1	9	(72,96,78)	5076	1
2	9	(43,97,77)	6087	2
3	3	(96,81,77)	4428	3

To study how relevant the number of streamlines is in the whole brain, tractograms of 500k and 1M streamlines were computed with the commands described in section 3.2 for one same subject. Figure 4.3 shows the number of streamlines per voxel of both tractograms. Three specific voxels were selected to study in more detail the importance

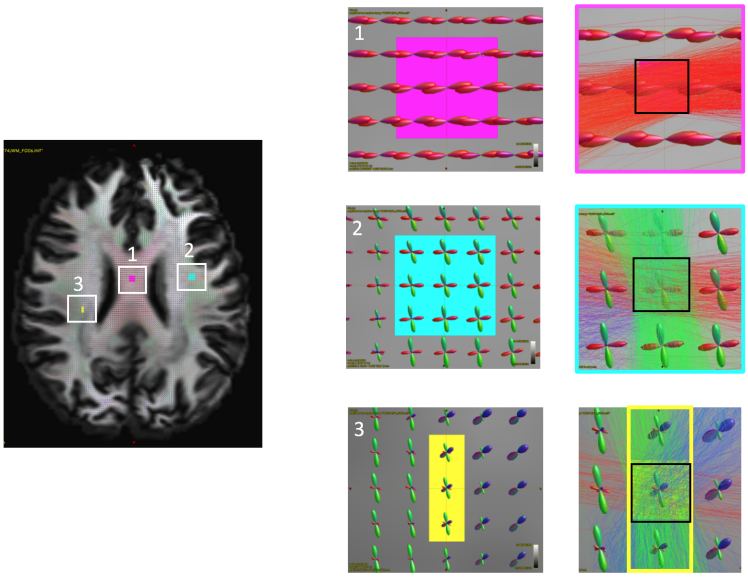

Figure 4.1: Streamlines crossing the central voxel of the regions 1,2 and 3 of the 10 million tractogram.

of the number of streamlines. Once again, the regions correspond to zones where the FOD lobes show one, two and three directions, respectively. In Table 4.2, comparison of the information of three voxels for both tractograms is presented. As expected, there are more streamlines in the 1M tractogram.

Table 4.2: Comparison of three regions of interest of 500k and 1M tractograms

Region	Voxel	Streamlines		Directions expected
		500k	1M	
1	(71,95,77)	1056	2224	1
2	(55,111,77)	688	1576	2
3	(94,85,77)	1144	2144	3

All the streamlines crossing the selected voxels are shown in Figure 4.2. A multiple representation of the distribution of the number of streamlines per voxel of 500k and 1M tractograms can be seen in Figure 4.3. It can be seen that the average of streamlines per voxel in the 1M tractogram is higher than in the 500k tractogram.

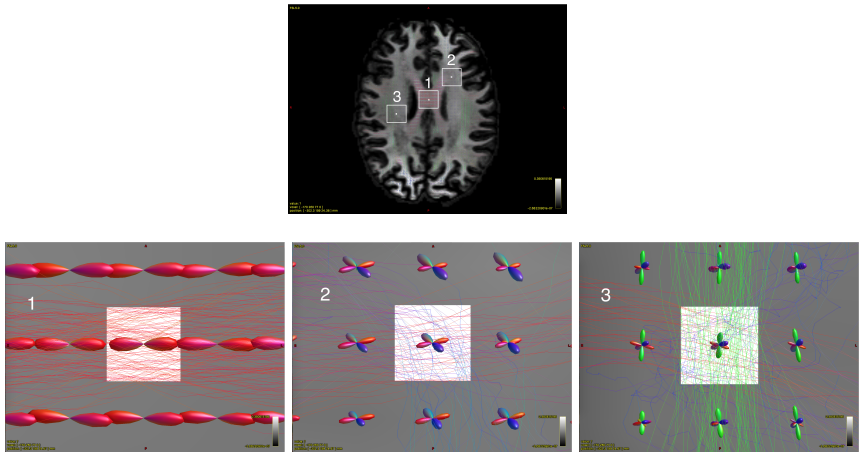

(a) 500k tractogram

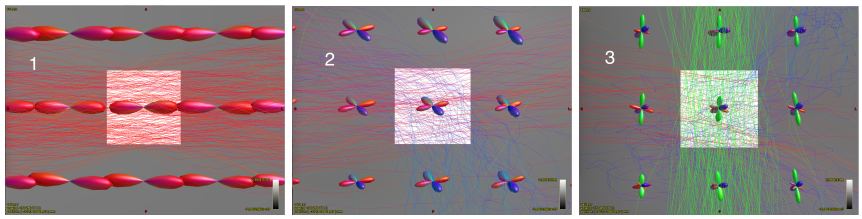

(b) 1M tractogram

Figure 4.2: Representation of the streamlines crossing the three selected voxels corresponding to regions with 1, 2 and 3 orientations, respectively, of the 500k (a) and 1M (b) tractograms. (Better seen in electronic format).

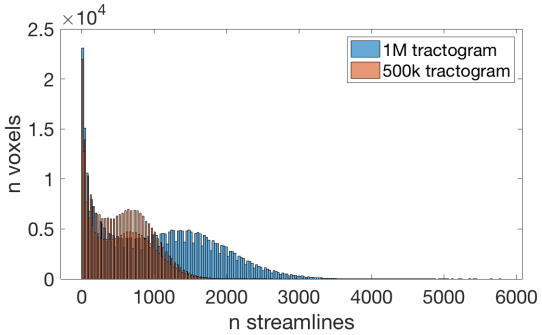

Figure 4.3: Number of streamlines per voxel of 500k tractogram (orange) and 1M tractogram (blue).

4.2 SIFT2

In order to understand the SIFT2 method, it was subsequently applied to the tractograms of both 500k and 1M streamlines computed before. For every voxel, the mean and standard deviation of all the SIFT2 values of all the streamlines were calculated and used to compare how those weights change with the variation of the number of streamlines. Results are shown in Figure 4.4. The local study of some pixels to check in detail the difference of the SIFT2 weights between the two tractograms is shown in Figure 4.5.

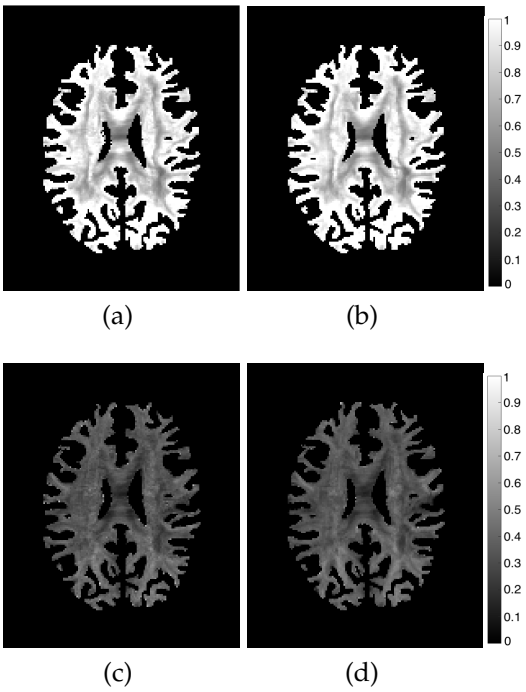

Figure 4.4: Representation of the mean and the standard deviation of the SIFT2 values per voxel. (a) and (b) show the mean for 500k and 1M tractogram, respectively, and (c) and (d) the standard deviation.

A possible relation between number of streamlines and SIFT2 values per voxel was studied. Figure 4.6 shows a representation of the number of streamlines per voxel of the 500k and 1M tractograms. Notice that they are not in the same scale since what it is of interest to study is the pattern they have according to the number of streamlines.

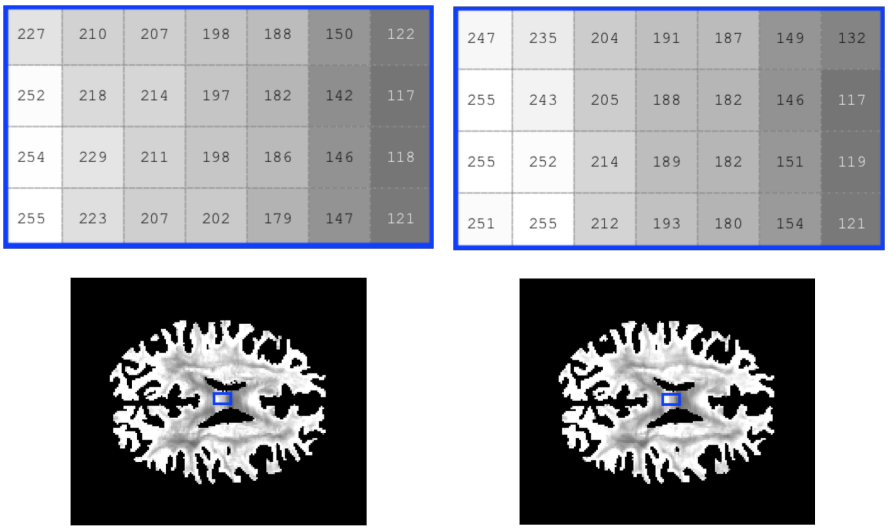

(a) 500k tractogram (b) 1M tractogram

Figure 4.5: Pixel values of SIFT2 of the 500k and 1M tractograms at a concrete area of the brain.

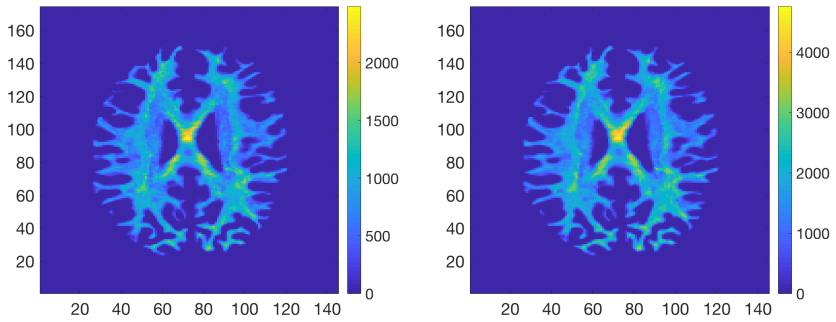

(a) 500k tractogram (b) 1M tractogram

Figure 4.6: Representation with a colormap of the average number of streamlines per voxel of each tractogram.

The patterns seen in Figure 4.6 seem very similar for both tractograms. In addition, these patterns seem to match with the ones in Figure 4.4, which could mean that there is a relation between SIFT2 values and the number of streamlines. To evaluate this hypothesis, linear regression was used. Results are presented in Figure 4.7.

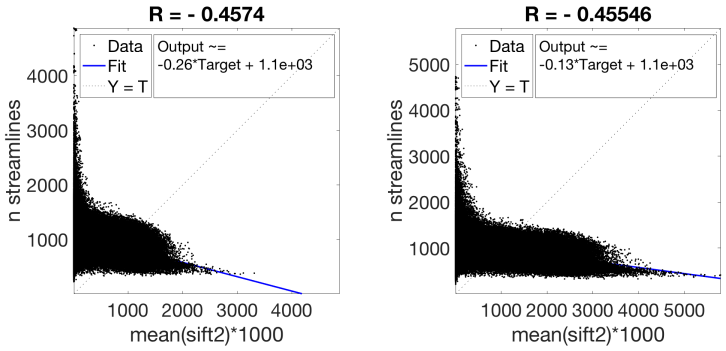

(a) 500k (b) 1M

Figure 4.7: Linear regression of number of streamlines and mean of the SIFT2 values, per voxel, of 500k and 1M tractograms.

Logistic regression was also used to carry out a comparison between the original SIFT and the SIFT2 methods, as Figure 4.8 shows. Moreover, Figure 4.9 shows the histogram of the SIFT2 values according to the values of SIFT.

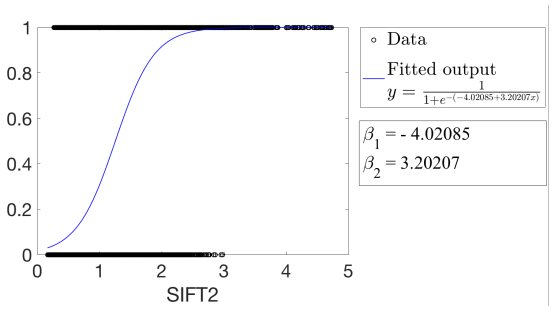

Figure 4.8: Logistic regression of SIFT and SIFT2 values. For SIFT, 0 means the streamline is removed and 1 means the streamline remains. The p-value shows strong significance in the relation between the two variables.

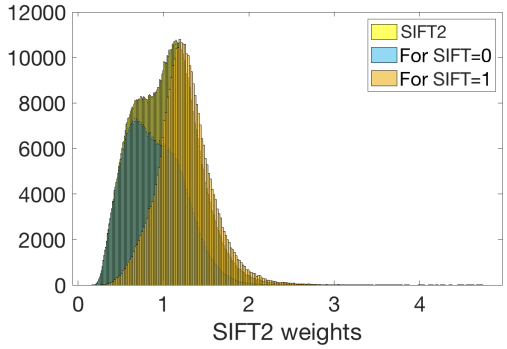

Figure 4.9: Representation of the distribution of SIFT2 values. In yellow, all the values. In blue, the SIFT2 values that correspond to the streamlines that SIFT removes when using SIFT. In orange, the SIFT2 values that correspond to the streamlines that SIFT does not remove when using SIFT.

4.3 Clustering

The central voxel of each region was selected to perform the two different clustering methods explained in section 3.5. Before the clustering, data was represented to analyze and speculate what to expect from the clustering. This can be seen in Figure 4.10. For the Mean Shift method, weights are required as an input, therefore, data was represented in a sphere giving separately both SIFT2 and curvature values as weights in order to check if they were providing some additional information. To compare them, the values of the weights were normalized, and the results are shown in Figure 4.11.

When performing the method of Brusini et al. [9], the streamlines were always clustered into one cluster. Instead, with the Mean Shift method, the number of clusters changed depending on the voxel. This latter method was performed with SIFT2 values given as weights and different values of κ parameter of the Von Mises-Fisher kernel (see equation 3.5) were tested. In Figure 4.12, it can be seen how the number of clusters vary with the variation of the κ parameter. Results for the Mean Shift method are presented in Figure 4.13, with $\kappa = 20$.

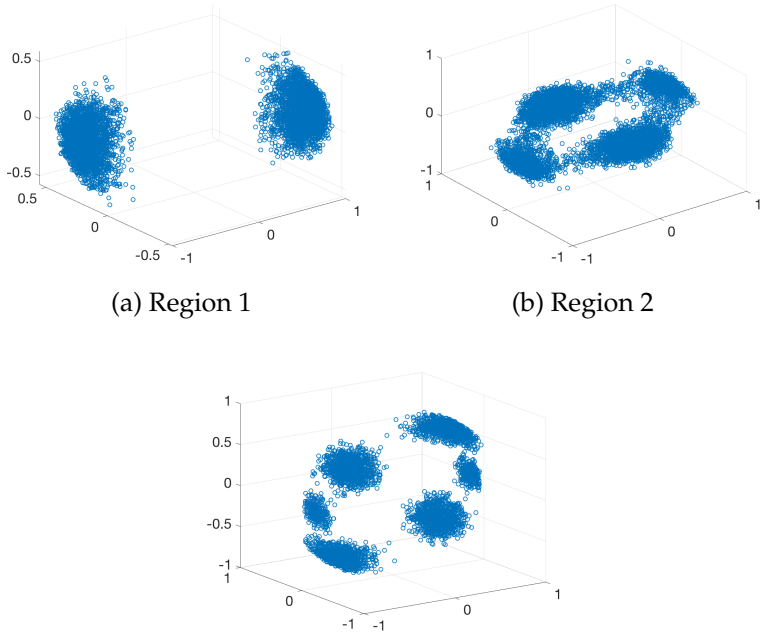

(a) Region 1

(b) Region 2

(c) Region 3

Figure 4.10: Representation data before clustering.

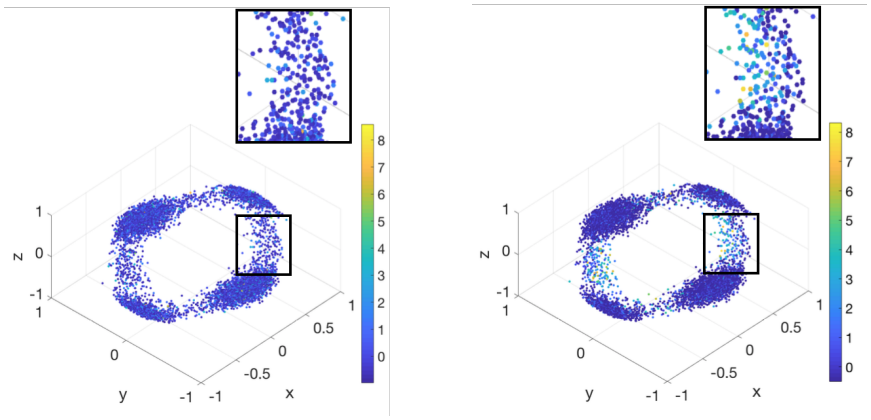

(a) SIFT2

(b) Curvature

Figure 4.11: Representation of the contribution of SIFT2 and Curvature values as weights.

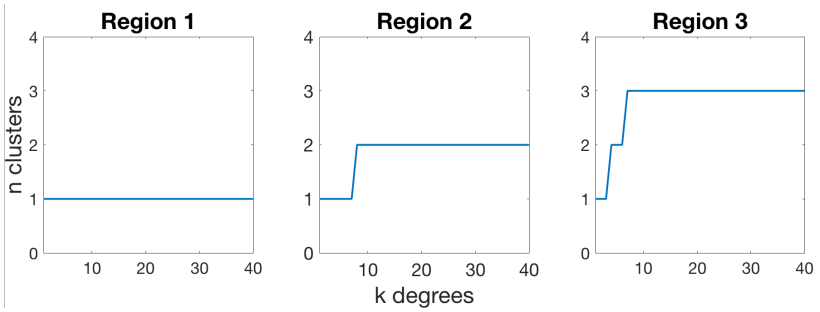

Figure 4.12: Number of clusters according to κ-values using Mean Shift method on the 10M tractogram.

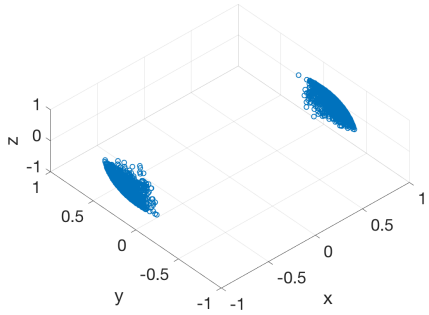

(a) Region 1

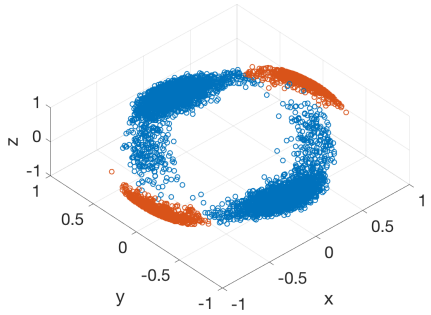

(b) Region 2

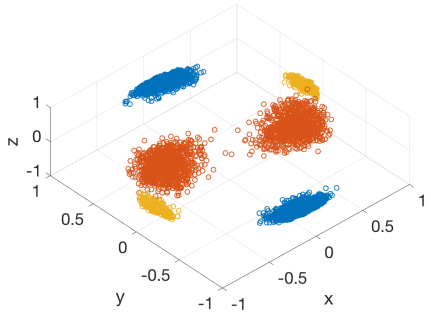

(c) Region 3

Figure 4.13: Clusters per region using Mean Shift algorithm on the 10 million tractogram.

Chapter 5

Discussion

In the present study, specific methods were selected and used to generate tractography data from which some features were extracted on a voxel-level to finally be able to cluster the fiber bundles of the WM.

5.1 Streamlines

Tractograms analyzed during this study had 500k, 1M and 10M streamlines. Figures 4.1 and 4.2 show that, in all the three cases, the tractograms correctly followed the directions represented by the FOD lobes. The regions of interest were selected from areas where there is evidence of the presence of crossing fibers as well as fibers following a single direction. It is definitely clear that, with the 10 million tractogram, the representation will be very accurate. On the other hand, the computational time and memory needed are extremely high. That is the reason why tractograms with less streamlines were generated for comparison. As it is shown in Table 4.2 and Figure 4.2, representations of the 500k tractogram may seem to be poor at some point, such as the region 2, whereas the ones of the 1M tractogram seem to be sufficient to represent the fiber population existing in those voxels. Figure 4.3 shows that most of the voxels in the 500k tractogram will have around 700 streamlines in average, whereas in the 1M tractogram they will have around 1500 tracts. If the 10 million tractogram was compared as well, the expected average number of streamlines will be around 4500. It was then proved that the number of streamlines to select when gen-

erating the tractogram is a non-trivial parameter and 1 million seems to be an appropriate number to get consistent results with reasonable computational time and efficiency.

5.2 SIFT2

The presence of possible relations between SIFT2 weights and other tractography parameters were investigated, in order to identify whether the method is able to add any useful information to the tractography dataset. From Figure 4.4, the mean and standard deviation of the SIFT2 values per voxel barely seem to differ between the different two tractograms. This is shown with more accuracy in Figure 4.5. Moreover, from Figure 4.6, a relation between the number of streamlines and the mean of the SIFT2 values per voxel seem to be present. The voxels represented in Figure 4.6 seem to have more streamlines at the regions where the mean values of the SIFT2 are lower, which was not expected. However, the linear regression analysis showed inconsistency with the prior hypothesis (R = - 0.4574 for 500k tractogram and R = - 0.45546 for 1M tractogram). It is true that there are voxels with low number of streamlines that have high weights and voxels with high number of streamlines that have low weights, but this pattern is not consistent for all voxels so it cannot be stated that there is any relation between the two. Logistic regression was used to compare both methods, which shows that they work in the same way since there is high significance in their relation (p-values < 0.0001). Lower SIFT2 weights were expected to correspond to the streamlines to which the original method gives a value of 0 and the opposite. Figure 4.8 corroborates that statement. However, it can be seen a non reliable region between the range of values 0.8 and 1.7. This region corresponds to the majority of streamlines which means that one can not use SIFT2 method expecting to get the same results as when using the original method. This can also be appreciated in Figure 4.9, where it can be seen a wide overlap between the group of SIFT2 weights that corresponds to the streamlines that SIFT removes and the group of SIFT2 weights that corresponds to the streamlines remaining using SIFT.

5.3 Clustering

From all the features extracted in the voxel-wise characterization, a study of the contribution of the curvature and SIFT2 values was carried out. The region 2 was the one selected to perform it because of the pattern the data follows: two cluster can be easily identified by simple visual inspection, but there are also some additional tracts that do not clearly belong to any of those two clusters. In Figure 4.11 it can be seen that the SIFT2 values barely change within the plotted tracts. However, when giving curvature values as weights, the above-mentioned points whose clusters are not evident have higher values than the rest of the data. This means the streamlines crossing that area more curved than the others.

When performing the method of Brusini et al. [9], the streamlines were always grouped into one cluster, questioning its effectiveness for this study. This can be explained due to the number of streamlines selected to generate the tractograms. The method was designed and worked successfully for 300k streamlines. Since this study was done with a 10M tractogram, which is more than triple, all the streamlines will be very close for the method and this will tend to group them all into one cluster.

The Mean Shift method proved promising results. The number of clusters of each region were the expected ones, but, while the patterns in regions 1 and 3 are clearly separable, the clustering of the above-mentioned high-curavutre data from region 2 is not as clear. Indeed, when visualizing the tractogram overlayed with the FOD lobes in Figure 4.1 it can be seen that in region 2 there are also a few additional tracts crossing the voxels along a different direction than the two main ones, which could explain the patterns presented in Figure 4.11. Different values of κ were tried to see whether this could decrease the restriction in the number of clusters and lead to the creation of a new cluster corresponding to the high-curvature points. However, as shown in Figure 4.12, the number of clusters was always equal to two for any tested κ>10. This suggests that assigning a value of 10 to the κ parameter can be a suitable choice for the presented clustering purpose.

Chapter 6

Conclusion

In this project, a procedure was defined to generate, characterize and cluster fiber geometries of WM at a local level. In order to achieve optimal results, different methods, configurations and parameters were analyzed using tractography data from subjects from the HCP. MSMT-CSD and probabilistic ACT were the methods selected to extract the FODs and generate the corresponding tractograms, on which the SIFT2 method was performed next.

Tractograms of three different number of streamlines were generated: 500.000, 1 million and 10 million. The three of them showed consistency with FOD directions but, while with 10 million the representation is very accurate, with 500.000 it is quite poor. On the other hand, 1 million seemed to be a sufficient number for the scope of this project.

This SIFT2 method did not cause any alteration of the results. A comparison between tractograms with different number of streamlines and SIFT2 values was carried out, but no evident differences were identified. The relation between the number of streamlines per voxel and SIFT2 weights was also studied. Visually, there seemed to be an indirectly proportional relationship, but using linear regression evaluation, it was proved that there was not any. In addition, it was seen that SIFT2 method works well for extreme values, which shows consistency with the original method. However, in the region of interest there is a wide overlap that does not provide enough reliability to use the method.

Regarding the clustering, the method used in previous studies of Brusini [8] does not seem to work properly with the amount of streamlines selected for this study. Instead, it has been proved that the Mean Shift algorithm could be used to distinguish the different bundles existing at every voxel of the investigated regions of interest. However, it did not provide any additional information for the clustering, suggesting that other parameters should be taken into account. For this reason, a possible next step would be to adapt the distance measurement function from the method of Brusini et al. [9] to the Mean Shift one, which also depends on the curvature angle of the tracts.

Bibliography

[1] D.C. Alexander. "Modelling, fitting and sampling in diffusion MRI". In: *Visualization and Processing of Tensor Fields, Springer* (2009), pp. 3–20.

[2] J.D. Tournier et al. "Direct estimation of the fiber orientation density function from diffusion-weighted MRI data using spherical deconvolution". In: *NeuroImage* 23 (2004), pp. 1176–1185.

[3] G. Gerig, S. Gouttard, and I. Corouge. "Analysis of brain white matter via fiber tract modeling". In: *Annual International Conference of the IEEE Engineering in Medicine and Biology Society* (2004).

[4] D. Pai, O. Muzik, and J. Hua. "Quantitative analysis of diffusion tensor images across subjects using probabilistic tractography". In: *15th IEEE International Conference on Image Processing* (2008).

[5] D. Xu et al. "A framework for callosal fiber distribution analysis". In: *Neuroimage* 17 (2002), pp. 1131–1143.

[6] T. Dhollander et al. "Track Orientation Density Imaging (TODI) and Track Orientation Distribution (TOD) based tractography". In: *NeuroImage* 94 (2014), pp. 312–336.

[7] I. Brusini et al. "Influence of tractography algorithms and settings on local curvature estimation". In: *Proceedings of OHBM Annual Meeting* (2017).

[8] I. Brusini. "Voxel-wise characterization of neural tract using tractography data". MA thesis. Stockholm, Sweden: Kungliga Tekniska Högskolan, 2016.

[9] I. Brusini et al. "Voxel-wise characterization of neural tracts using tractography data". In: *Proceedings of CDMRI* (2018).

[10] WU-Minn Consortium Human Connectome Project. "WU-Minn HCP 500 Subjects Data Release: Reference Manual". In: *Proceedings of OHBM Annual Meeting* (2014).

[11] L. W. Swanson. *Basic Principles of Nervous System Organization*. English. Neuroscience in the 21st Century: From Basic to Clinical, 2013, pp. 1255–1288.

[12] J. Gili. *Introducción biofísica a la resonancia magnética en neuroimagen*. Spanish. Barcelona, Spain, 2009.

[13] RR. Edelman RR and J. Hesselink. *Clinical magnetic resonance imaging*. English. Saunders Publishing Co, 1990.

[14] D. K. Jones. *Diffusion MRI Theory, Methods, and Applications*. English. Oxford University Press, 2010.

[15] S. Mori and J. Tournier. *Introduction to diffusion tensor imaging: And higher order models: Second edition*. English (US). Elsevier Inc., Sept. 2013. ISBN: 9780123983985.

[16] J. I. Berman et al. "High Angular Resolution Diffusion Imaging (HARDI) Probabilistic Tractography of the Auditory Radiation". In: *AJNR. American journal of neuroradiology* 34 (2013), pp. 1573–1578.

[17] J.D. Tournier, F. Calamante, and A. Connelly. "Robust determination of the fibre orientation distribution in diffusion MRI: Non-negativity constrained super-resolved spherical deconvolution". In: *NeuroImage* 35 (2007), pp. 1459–1472.

[18] T.E.J. Behrens et al. "Probabilistic diffusion tractography with multiple fibre orientations: What can we gain?" In: *NeuroImage* 34 (2007), pp. 144–155.

[19] B. Jeurissen et al. "Investigating the prevalence of complex fiber configurations in white matter tissue with diffusion MR". In: *Hum. Brain Mapp* (2012).

[20] A. Lemkaddem et al. "Global tractography with embedded anatomical priors for quantitative connectivity analysis". In: *Front Neurol* 35 (2014), pp. 1459–1472.

[21] R.E. Smith et al. "Anatomically-constrained tractography: Improved diffusion MRI streamlines tractography through effective use of anatomical information". In: *NeuroImage* 62 (2012), pp. 1924–1938.

[22] R.E. Smith et al. “SIFT: Spherical-deconvolution informed filtering of tractograms”. In: *NeuroImage* 67 (2013), pp. 298–312.

[23] R.E. Smith et al. “SIFT2: Enabling dense quantitative assessment of brain white matter connectivity using streamlines tractography”. In: *NeuroImage* 119 (2015), pp. 338–351.

[24] V. Siless et al. “AnatomiCuts: Hierarchical clustering of tractography streamlines based on anatomical similarity”. In: *NeuroImage* 166 (2018), pp. 32–45.

[25] A. K. Jain, M. N. Murty, and P. J. Flynn. “Data Clustering: A Review”. In: *ACM Comput. Surv.* 31.3 (1999), pp. 264–323.

[26] J. Wasserthal, P. Neher, and K. Maier-Hein. “TractSeg - Fast and accurate white matter tract segmentation”. In: *NeuroImage* 183 (2018), pp. 239–253.

[27] J.D. Tournier, F. Calamante, and A. Connelly. “Diffusion Tractography in Crossing Fiber Regions”. In: *International Journal of Imaging Systems and Technology,* 22 (2012), pp. 53–66.

[28] B. Jeurissen et al. “Multi-tissue constrained spherical deconvolution for improved analysis of multi-shell diffusion MRI data”. In: *NeuroImage* 103 (2014), pp. 411–426.

[29] D. L. Davies and D. W. Bouldin. “A Cluster Separation Measure”. In: *IEEE Transactions on Pattern Analysis and Machine Intelligence* 1 (1979), pp. 224–227.

[30] K. Fukunaga and L. Hostetler. “The estimation of the gradient of a density function, with applications in pattern recognition”. In: *IEEE Transactions on Information Theory* 21.1 (1975), pp. 32–40.